Advanced Steel Construction – Vol. 17 No. 3 (2021) 231–242
DOI:10.18057/IJASC.2021.17.3.2

FINITE ELEMENT ANALYSIS OF UNFASTENED COLD-FORMED STEEL CHANNEL SECTIONS WITH WEB HOLES UNDER END-TWO-FLANGE LOADING AT ELEVATED TEMPERATURES

Ankur Kumar [1], Krishanu Roy [2, *], Asraf Uzzaman [3] and James B.P. Lim [2]

[1] *Department of Mechanical Engineering, Indian Institute of Technology Delhi, India*
[2] *Department of Civil and Environmental Engineering, The University of Auckland, New Zealand*
[3] *School of Computing, Engineering and Physical Sciences, University of the West of Scotland, Paisley, PA1 2BE, United Kingdom*
** (Corresponding author: E-mail: kroy405@aucklanduni.ac.nz)*

ABSTRACT

This paper presents the results of a finite element investigation on cold-formed steel (CFS) channel sections with circular web holes under end-two-flange (ETF) loading condition and subjected to elevated temperatures. The stress strain curve for G250 CFS with 1.95 mm thickness at elevated temperatures was taken from Kankanamge and Mahendran and the temperatures were considered up to 700 oC. To analyse the effect of web hole size and bearing length on the strength of such sections at elevated temperatures, a parametric study involving a total of 288 FE models was performed. The parametric study results were then used to assess the applicability of the strength reduction factor equation presented by Uzzaman et al. for CFS channel-sections with web holes under ETF loading from ambient temperature to elevated temperatures. It is shown that the reduction factor equation is safe and reliable at elevated temperatures.

ARTICLE HISTORY

Received: 30 June 2020
Revised: 9 February 2021
Accepted: 28 February 2021

KEYWORDS

Cold-formed steel;
Channel sections;
End-two-flange;
Web crippling;
Finite element analysis;
Elevated temperatures;
Web holes

1. Introduction

Cold-formed steel (CFS) sections are used increasingly in commercial and residential buildings because of its superior strength to weight ratio, and ease of installation [1-4]. These sections usually have web holes for installation of electrical and plumbing services.

Web crippling is a well-known problem associated with these CFS sections, particularly when these sections are subjected to concentrated load near the web holes. This problem is exacerbated when such sections are subjected to elevated temperatures.

Significant information is available in the literature for design guidance of CFS channel-sections, to be referred to as C sections, at ambient temperature under web crippling [5-10]. However, limited research is available on the web crippling capacity of such perforated CFS channel sections subject to concentrated load near the holes and under elevated temperatures. This lack of design information for C-sections at elevated temperatures makes it difficult for practising engineers and researchers to predict the web crippling capacity of C-sections under elevated temperatures.

Recently published research studies have focussed on the material behaviour of CFS sections at elevated temperatures. Imran et al. [11] recently proposed a set of equations to evaluate the mechanical property reduction factors for square, rectangular and circular CFS hollow sections at elevated temperatures. Coupons were cut from such hollow sections with temperatures ranging from 20^o C to 800^o C under steady state condition. The aim was to determine the reduction in material properties. Kankanamge and Mahendran [12] also proposed equations to predict the material property reduction factors and the stress-strain relationship of low and high strength steel (different grades and thicknesses) at elevated temperatures. A similar study was then reported by Ranawaka and Mahendran [13], who proposed empirical equations in order to determine the stress-strain relationship of both the high and low strength steels at elevated temperatures. Furthermore, Chen and Young [14] reported data for mechanical properties of G550 and G450 grades of CFS sections under both the steady and transient temperature conditions. Lim and Young [15] used the stress-strain relationships determined from the equations of Chen and Young [14] and investigated the behaviour of CFS bolted connections at elevated temperatures.

Alongside understanding the change in mechanical properties of CFS sections at elevated temperatures, researchers are also focussing on understanding the structural behaviour of different CFS sections at elevated temperatures. A number of investigations have been carried out to determine the effect of elevated temperatures on CFS beams. Landesmann and Camotim [16] presented a FE investigation on the distortional buckling behaviour of CFS C-sections under elevated temperatures. Laim et al. [17] studied the structural behaviour of C-sections loaded under elevated temperatures. Kankanamge and Mahendran [18] presented a study using a validated FE model to determine the structural behaviour of CFS lipped C-sections under bending at elevated temperatures.

A number of studies have also been reported in the literature which investigated the behaviour of CFS columns at elevated temperatures. Gunalan et al. [19] studied the local buckling behaviour of CFS lipped and unlipped C-sections under simulated fire loadings. Gunalan et al. [19] also presented a study on flexural-torsional buckling capacity of CFS lipped C-sections at ambient and elevated temperatures. Ranawaka and Mahendran [20] presented a study to determine the distortional buckling strength of CFS lipped C-sections at elevated temperatures. Chen and Young [14] conducted a numerical study to understand the behaviour of CFS lipped C-sections at elevated temperatures. Feng and Wang [21] presented a study to evaluate the axial strength of CFS C-sections under ambient and elevated temperatures.

It is to be noted that most of the research studies available in the literature focussed on the behaviour of CFS sections under compression and torsional loadings and not even a single research is available in the literature which investigated the effects of web holes on the web crippling strength of CFS C-sections under ETF loading conditions and at elevated temperatures. Furthermore, the current design specifications such as ASCE [22], EC3 [23] and BS5950 [24] do not provide any guidelines for CFS C-sections with web holes at elevated temperatures under web crippling. The issue is addressed in this paper.

Fig. 1 shows the definition of symbols used for the dimensions of the C-sections considered in this study. AS/NZ:4600 [25] offers reduction factor equations for C-sections with web holes. However, these equations focus on C-sections with web holes offset to the bearing edge and applicable only at normal temperature.

The main objective of this study is to determine the feasibility of the design equations proposed in the literature for CFS C-sections with web holes at ambient temperature to be used at elevated temperatures. The strength reduction factor proposed by Uzzaman et al. [26] for determining the web crippling capacity of unfastened CFS C-sections with centred web holes under ETF loading at ambient temperature, is as follows:

$$R = 0.90 + 0.12(N/h) - 0.60(a/h) \leq 1 \quad (1)$$

The limits for equation 1 are: $h/t \leq 156$, $N/h \leq 0.63$, $a/h \leq 0.8$, $N/t \leq 84$ and $\theta = 90^0$. Where, h is the depth of the flat portion of the web, t is the thickness, N is the bearing length, and a is the web-hole diameter.

Equation (1), however, is applicable at ambient temperature and there is no information available in the literature on whether this equation can be used for elevated temperature too. This paper considers if the same reduction factor equation is applicable to G250 grade of CFS C-sections subjected to ETF-loading at elevated temperatures. Kankanamge and Mahendran [12] provided the stress-strain curves of G250 grade of CFS sections with 1.95 mm thickness at elevated temperatures (Fig. 2). These stress-strain curves were adopted in the present study.

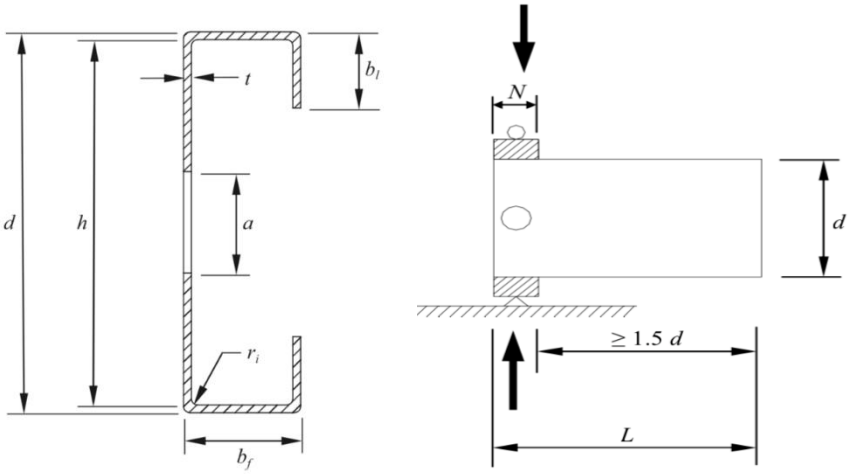

Fig. 1 Definition of symbols

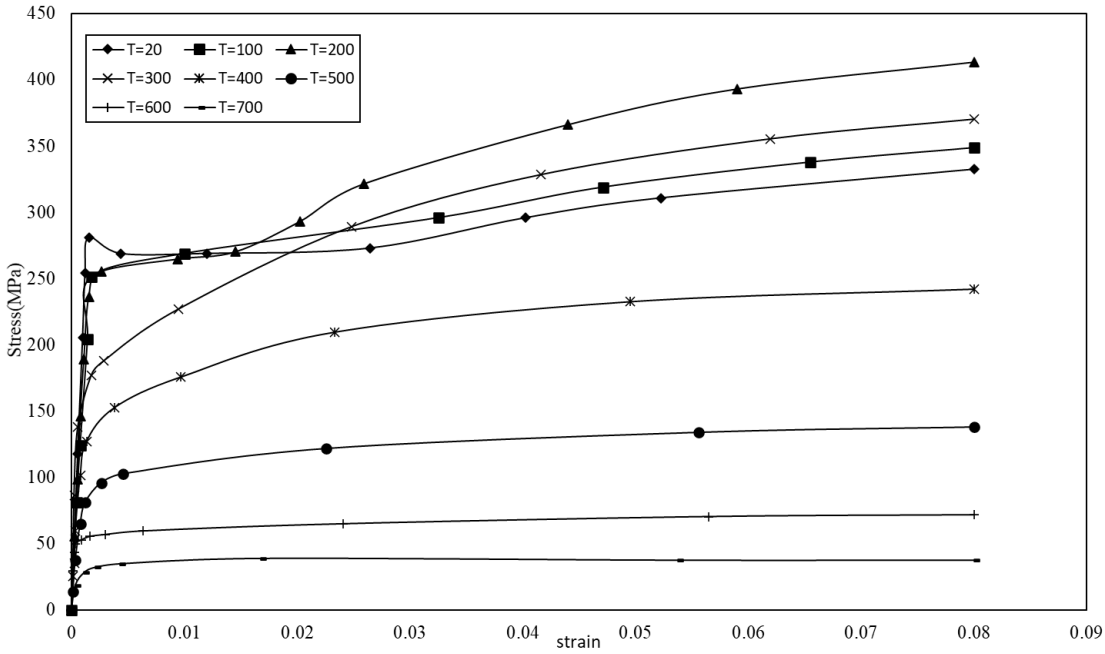

Fig. 2 Stress-strain curves (Kankanamge and Mahendran [12])

(a) centred circular web hole (b) offset circular web hole

Fig. 3 Experimental analysis of lipped CFS C-sections (unfastened flanges) under ETF loading condition from Uzzaman et al. [26]

2. Experimental investigation

Uzzaman et al. [27] conducted 44 experimental tests on lipped C-sections with web holes under ETF loading condition (Fig. 3). Web hole size was varied

in order to determine its effect on web crippling strength of such sections. Five different specimens were used with varying parameters such as nominal thickness, web depth, flange width, and web slenderness (h/t). To validate the developed nonlinear FE model (details are given in Uzzaman et al. [27]), laboratory test results were used. The validated FE model was then used to determine the strength reduction factor for CFS C-sections with web holes under ETF loading condition. More details of the experimental study can be found in Uzzaman et al. [27].

3. Numerical investigation

3.1. General

The general-purpose finite element software ANSYS [28] was used to develop a finite element model for CFS C-sections with web holes under elevated temperatures and subject to web crippling. The bearing plates, C-sections with and without the web holes and the interface between the lipped C-sections and bearing plates were modelled appropriately. More details of the FE model are summarised in the following sections.

3.2. Specimen Labelling

The dimensions of the C-sections are presented in Table 1. Fig. 1 shows the definition of symbols used for the dimensions of C-sections considered in this study. The specimens were labelled in such a way that the loading condition, specimen dimensions, bearing length as well as the (a/h) ratio can be identified by the specimen label. For example, the label "ETF100 x 40 x 15 x 5 t-1.95 N50" can be explained as follows:

- The first notation 'ETF' indicates the loading condition which is End-two flange loading.
- The next three notations define the nominal dimensions of the C-section: '100 x 40 x 15' indicates the nominal depth, flange width and overall lip width of the section in millimetres.
- 't-1.95' indicates the thickness of the C-section; and
- 'N50' shows the bearing length (i.e. 50mm).
- The notation 'A0.4' indicates the value of (a/h) ratio as 0.4. 'A0' denotes the C- sections without web holes. Only unfastened flanges were considered in this study.

Table 1
Dimension of specimens considered in the study

Specimen	Web d(mm)	Flange b_f(mm)	Lip h_l(mm)	Length L(mm)	Thickness t(mm)	Fillet r_i(mm)	Web depth h(mm)	Web slenderness h/t	Bearing length N(mm)	Bearing Length ratio N/h	Web hole Ratio a/h	Diameter of web hole a(mm)
ETF100x40x15-t-1.95N50A0	100	40	15	350	1.95	5	98.1	50.3	50	0.51	0	0
ETF100x40x15t-1.95N50A0.4	100	40	15	350	1.95	5	98.1	50.3	50	0.51	0.4	39.22
ETF100x40x15-t-1.95N75A0	100	40	15	375	1.95	5	98.1	50.3	75	0.76	0	0
ETF100x40x15-t-1.95N75A0.4	100	40	15	375	1.95	5	98.1	50.3	75	0.76	0.4	39.22
ETF 125x40x15-t-1.95N50A0	125	40	15	425	1.95	5	123.1	63.1	50	0.41	0	0
ETF 125x40x15-t-1.95N50A0.4	125	40	15	425	1.95	5	123.1	63.1	50	0.41	0.4	49.22
ETF 125x40x15-t-1.95N50A0.6	125	40	15	425	1.95	5	123.1	63.1	50	0.41	0.6	73.83
ETF 125x40x15-t-1.95N50A0.8	125	40	15	425	1.95	5	123.1	63.1	50	0.41	0.8	98.44
ETF 125x40x15-t-1.95N75A0	125	40	15	450	1.95	5	123.1	63.1	75	0.61	0	0
ETF 125x40x15-t-1.95N75A0.4	125	40	15	450	1.95	5	123.1	63.1	75	0.61	0.4	49.22
ETF 125x40x15-t-1.95N75A0.6	125	40	15	450	1.95	5	123.1	63.1	75	0.61	0.6	73.83
ETF 125x40x15-t-1.95N75A0.8	125	40	15	450	1.95	5	123.1	63.1	75	0.61	0.8	98.44
ETF 125x40x15-t-1.95N100A0	125	40	15	475	1.95	5	123.1	63.1	100	0.81	0	0
ETF 125x40x15-t1.95N100A0.4	125	40	15	475	1.95	5	123.1	63.1	100	0.81	0.4	49.22
ETF 125x40x15-t1.95N100A0.6	125	40	15	475	1.95	5	123.1	63.1	100	0.81	0.6	73.83
ETF 125x40x15-t1.95N100A0.8	125	40	15	475	1.95	5	123.1	63.1	100	0.81	0.8	98.44
ETF 150x40x15-t-1.95N50A0	150	40	15	500	1.95	5	148.1	75.9	50	0.34	0	0
ETF 150x40x15-t-1.95N50A0.4	150	40	15	500	1.95	5	148.1	75.9	50	0.34	0.4	59.22
ETF 150x40x15-t-1.95N50A0.6	150	40	15	500	1.95	5	148.1	75.9	50	0.34	0.6	88.83
ETF 150x40x15-t-1.95N50A0.8	150	40	15	500	1.95	5	148.1	75.9	50	0.34	0.8	118.44
ETF 150x40x15-t-1.95N75A0	150	40	15	525	1.95	5	148.1	75.9	75	0.51	0	0
ETF 150x40x15-t-1.95N75A0.4	150	40	15	525	1.95	5	148.1	75.9	75	0.51	0.4	59.22
ETF 150x40x15-t-1.95N75A0.6	150	40	15	525	1.95	5	148.1	75.9	75	0.51	0.6	88.83
ETF 150x40x15-t-1.95N75A0.8	150	40	15	525	1.95	5	148.1	75.9	75	0.51	0.8	118.44
ETF 150x40x15-t-1.95N100A0	150	40	15	550	1.95	5	148.1	75.9	100	0.68	0	0
ETF 150x40x15-t1.95N100A0.4	150	40	15	550	1.95	5	148.1	75.9	100	0.68	0.4	59.22
ETF 150x40x15-t1.95N100A0.6	150	40	15	550	1.95	5	148.1	75.9	100	0.68	0.6	88.83
ETF 150x40x15-t1.95N100A0.8	150	40	15	550	1.95	5	148.1	75.9	100	0.68	0.8	118.44

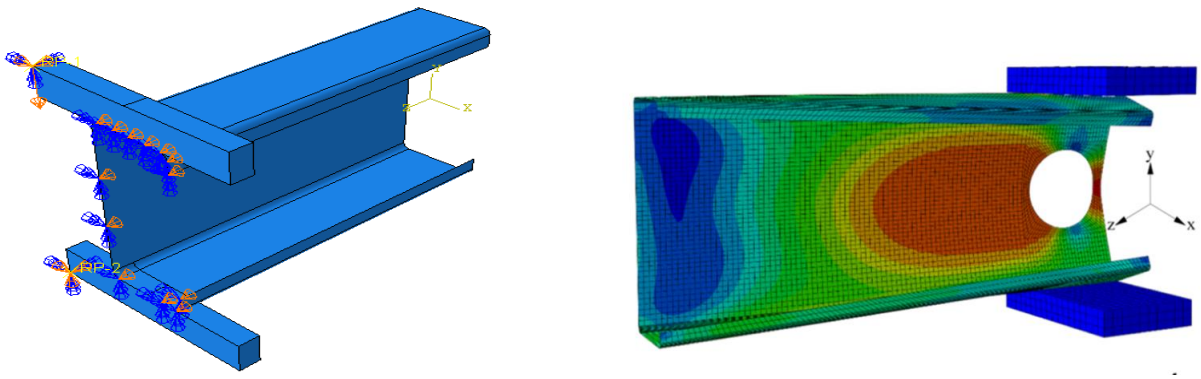

Fig. 4 a) Boundary conditions applied in the FEA model for ETF-100x45x15-t1.95N50A0 b) Deformed shape predicted by the FEA model for ETF-125x45x15t1.95N100A0.4

3.3. Mesh sensitivity and element type

Fig. 4 shows the FE mesh of the C-sections and the bearing plate. As the number of elements in the FE mesh increases, the accuracy of the results increases. In order to obtain the results within the acceptable limits, very fine mesh sizes were used for all the FE models developed in this study. The mesh sizes were varied from 3mm x 3mm (width by length) to 5mm x 5mm, based on the computational time and accuracy of the results.

In order to incorporate corner strength enhancements of CFS C-sections, it is important to use finer meshing at the corners of C-sections. The number of FE elements in the corner between the web and flange was chosen as 9. This value was maintained at 3, while modelling the corners of lip and the flange. The regions near the web holes were finely meshed. To optimise the mesh size and its numbers, mesh sensitivity analysis was performed.

Four-noded shell element SHELL 181 available in theANSYS library [28] was used to model the C-sections. Eight-noded solid element SOLID45 was used to model the bearing plates. In order to model the surface interface between the flanges and the bearing plates, CONTAT173 and TARGET170 elements were used.

Table 2
Material properties of G250 grade of CFS having a section thickness of 1.95 mm (Kankanamge and Mahendran [12])

Temp (°C)	σu (T) (MPa)	E(Mpa)	fy(Mpa)
20	356.1	188220	270.5
100	369.0	179640	267.3
200	435.2	171745	257.0
300	385.0	154330	196.4
400	240.0	121230	147.7
500	137.5	90631	95.8
600	71.4	57777	54.1
700	37.7	31363	34.4

3.4. Material and Geometry Properties

The FE model used in this study was developed by Uzzaman et al. [27] for CFS C-channels at ambient temperature (Fig. 3). The stress-strain curves of 1.95mm thick G250 grade of CFS C-sections at elevated and ambient temperatures were taken from the Kankanamge and Mahendran [12] (Fig. 2) and used in this study. The considered material properties are summarised in Table 2. Equations 2 and 3 were used to convert the engineering stress-strain relationship to the true stress-strain relationship as described in the ANSYS manual [28].

$$\sigma_{true} = \sigma_{eng}(\varepsilon_{eng} + 1) \tag{2}$$

$$\varepsilon_{true} = \ln(\varepsilon_{eng} + 1) \tag{3}$$

3.5. Loading and Boundary Condition

The surface-to-surface interaction was modelled between the load bearing plates and the flanges of C-sections using the surface contact option available in the ANSYS library [28]. The two contact surfaces were constrained to avoid any penetration between the two surfaces. Displacement control was used to apply the vertical load to the C-sections.

3.6. Verification of the FE Model

The results of FE analysis for CFS lipped C-sections with centred web holes subjected to ETF loading are presented in Table 3. The ratio of the load per web determined from the FEA and experiments shows good agreement between each other. For further verification purpose, the load displacement curves of specimen ETF142x60x13t-1.3N120 with a/h ratios ranging from 0 to 0.4 generated by FEA analysis was compared with the load displacement curve of same specimen obtained from the experimental study (Fig. 5). From the comparison, it was found that the FEA results were very close to the experimental results, confirming the validity of the FE model.

Table 3
Comparison of finite element analysis with the experiment results for flanges unfastened under ETF loading condition

Specimen	Web d	Flange b_f	Lip b_l	Thickness t	Fillet r_i	Holes a	Length L	Exp. load per web P_{EXP}	Web Crippling Strength per web predicted from P_{FEA}	Comparison P_{EXP}/P_{FEA}
	(mm)	(mm)	(mm)	(mm)	(mm)	(mm)	(mm)	(kN)	(kN)	
ETF142x60x13-t1.3N90A0	142.2	58.6	15.9	1.23	4.8	0.0	337.5	2.21	2.18	1.01
ETF142x60x13-t1.3N90A0.2	142.2	58.6	15.9	1.23	4.8	27.9	337.5	1.98	1.94	1.02
ETF142x60x13-t1.3N90A0.4	142.2	59.5	16.3	1.25	4.8	55.8	337.5	1.62	1.69	0.96
ETF142x60x13-t1.3N90A0.6	142.2	59.5	16.3	1.25	4.8	83.6	337.5	1.32	1.41	0.94
ETF172x65x13-t1.3N120A0	172.8	64.1	15.6	1.27	5.0	0.0	400.0	2.37	2.28	1.04
ETF172x65x13-t1.3N120A0.4	172.3	63.6	15.5	1.27	5.0	67.6	400.0	1.70	1.81	0.94
ETF172x65x13-t1.3N120A0.6	172.6	64.3	15.3	1.28	5.0	101.6	400.0	1.36	1.48	0.92
ETF202x65x13-t1.4N120A0	202.1	63.1	17.5	1.45	5.0	0.0	425.0	2.70	2.87	0.94
ETF202x65x13-t1.4N120A0.2	202.7	64.3	16.3	1.45	5.0	39.8	425.0	2.41	2.46	0.98
ETF202x65x13-t1.4N120A0.4	202.4	64.2	16.5	1.45	5.0	79.5	425.0	1.88	2.01	0.94
ETF202x65x13-t1.4N150A0	202.1	63.1	17.5	1.45	5.0	0.0	450.0	2.84	3.29	0.86
ETF202x65x13-t1.4N150A0.4	202.7	64.3	16.3	1.45	5.0	79.5	450.0	2.19	2.35	0.93
ETF202x65x13-t1.4N150A0.6	202.4	64.2	16.5	1.45	5.0	119.5	450.0	1.77	1.90	0.93

4. Parametric study

In this study, 288 FE models of C-sections with and without web holes with varying parameters such as sizes of web holes, bearing length and temperature ranging from 20 ^{0}C to 700 ^{0}C at an interval of 100 degrees were analysed. The aim of this parametric study was to investigate the effects of such parameters on the web crippling strength of CFS C-sections with web hole at elevated temperatures subjected to ETF crippling.

Lian et al. [6-7] and Uzzaman et al. [26] showed that the web crippling strength depends on the a/h ratio, and N/h ratio. To determine the effects of a/h ratio and N/h ratio at different elevated temperatures on the web crippling strength of CFS C-sections with web holes, a parametric study was conducted. In the parametric study, different web hole sizes and different bearing plate lengths were considered. Three different cross-sections were considered which include C100, C125 and C150 sections which had nominal depths of 100, 125 and 150 mm, respectively. Three different bearing plate lengths of 50mm, 75mm and 100mm were considered. The (a/h) ratio were varied as 0, 0.4, 0.6 and 0.8. The inside corner radius between the hole and the web were 5mm. For every specimen, the web crippling strength at different N/h ratio and a/h ratio at particular elevated temperature was obtained and summarised in Tables 5(a), 5(b) and 5(c). Thus, the strength reduction factor © at temperatures ranging from 20 degrees to 700 degrees is presented in Tables 5(a), 5(b) and 5(c). After

obtaining the reduction factor values for every particular temperature, the reduction factor values were compared with the reduction factor values predicted using the equation of Uzzaman et al. [26] (see Tables 5(a), 5(b) and 5(c), and Figs. 7(a) and 7(b)).

Fig. 6(a) presents the variation of strength reduction factor with the a/h ratio. Fig. 6(b) presents the variation of strength reduction factor with the N/h ratio. It was found that the strength reduction is insensitive to the N/h ratio for temperatures ranging from 20^0 C to 700^0 C.

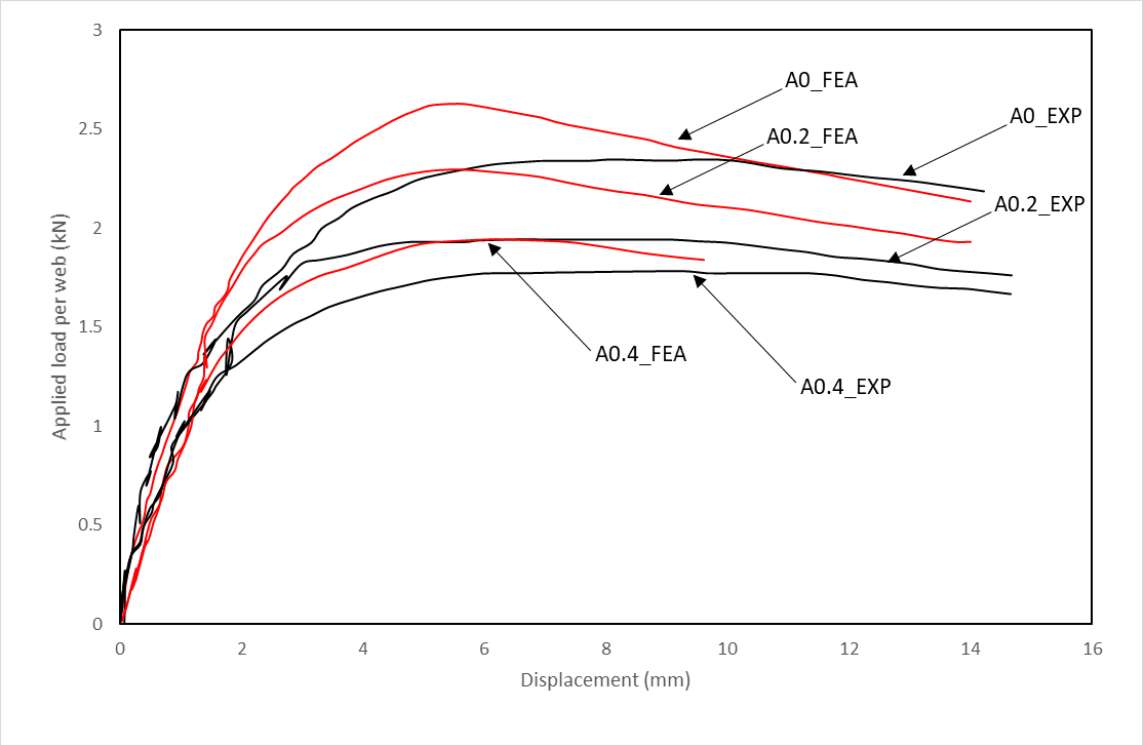

Fig. 5 Comparison of web deformation curves for ETF142x60x13t-13N120 from experiments and FEA

Table 4
Web crippling strengths of CFS C-sections at elevated temperatures
4(a) ETF100x45x15-t1.95

			FEA Load per Web (kN) at (a/h)			
Temperature(°C)	N(mm)	N/h	A0	A0.4	A0.6	A0.8
20			4.12	3.13	2.66	2.24
100			3.84	3.02	2.60	2.22
200			4.35	3.33	2.87	2.43
300	50	0.51	3.23	2.50	2.15	1.82
400			2.61	2.02	1.74	1.47
500			1.85	1.43	1.23	1.04
600			1.13	0.87	0.75	0.64
700			0.62	0.48	0.41	0.35
20			4.97	3.85	3.35	2.88
100			4.60	3.68	3.23	2.79
200			5.25	4.08	3.57	3.10
300			3.90	3.07	2.68	2.32
400	75	0.76	3.14	2.48	2.16	1.87
500			2.21	1.74	1.53	1.32
600			1.34	1.06	0.93	0.81
700			0.74	0.58	0.51	0.44
20			5.82	4.62	4.09	3.56
100			5.35	4.37	3.88	3.38
200			6.16	4.90	4.32	3.77
300			4.59	3.69	3.25	2.83
400	100	1.02	3.68	2.96	2.62	2.28
500			2.57	2.07	1.84	1.61
600			1.56	1.25	1.12	0.98
700			0.87	0.69	0.62	0.54

4(b) ETF125x45x15-t1.95

			FEA Load per Web (kN) at (a/h)			
Temperature(°C)	N(mm)	N/h	A0	A0.4	A0.6	A0.8
20			3.80	2.85	2.38	1.94
100			3.63	2.77	2.34	1.93
200			4.08	3.02	2.54	2.07
300			2.98	2.23	1.87	1.53
400	50	0.41	2.43	1.83	1.54	1.26
500			1.76	1.32	1.12	0.92
600			1.08	0.81	0.69	0.56
700			0.59	0.44	0.37	0.30
20			4.49	3.41	2.91	2.46
100			4.26	3.29	2.83	2.42
200			4.83	3.61	3.08	2.62
300			3.54	2.67	2.28	1.93
400	75	0.61	2.87	2.18	1.87	1.59
500			2.06	1.57	1.36	1.15
600			1.27	0.96	0.83	0.71
700			0.69	0.52	0.45	0.38
20			5.21	4.02	3.48	2.99
100			4.92	3.85	3.35	2.89
200			5.63	4.27	3.68	3.16
300			4.14	3.16	2.72	2.33
400	100	0.81	3.34	2.57	2.22	1.91
500			2.38	1.85	1.61	1.39
600			1.46	1.13	0.99	0.85
700			0.80	0.62	0.53	0.46

4(c) ETF150x45x15-t1.95

			FEA Load per Web (kN) at (a/h)			
Temperature(°C)	N(mm)	N/h	A0	A0.4	A0.6	A0.8
20			3.53	2.62	2.16	1.72
100			3.45	2.56	2.13	1.71
200			3.83	2.76	2.28	1.81
300			2.77	2.01	1.66	1.32
400	50	0.34	2.28	1.67	1.38	1.10
500			1.67	1.23	1.03	0.82
600			1.04	0.76	0.63	0.50
700			0.56	0.41	0.34	0.27
20			4.09	3.07	2.58	2.14
100			3.98	2.99	2.53	2.11
200			4.45	3.24	2.71	2.24
300			3.23	2.37	1.98	1.64
400	75	0.51	2.65	1.96	1.64	1.36
500			1.93	1.44	1.22	1.01
600			1.20	0.89	0.75	0.62
700			0.64	0.48	0.40	0.33
20			4.69	3.56	3.02	2.56
100			4.56	3.45	2.95	2.51
200			5.13	3.76	3.19	2.68
300			3.73	2.76	2.33	1.96
400	100	0.68	3.05	2.27	1.93	1.63
500			2.21	1.66	1.42	1.21
600			1.37	1.02	0.88	0.74
700			0.74	0.55	0.47	0.40

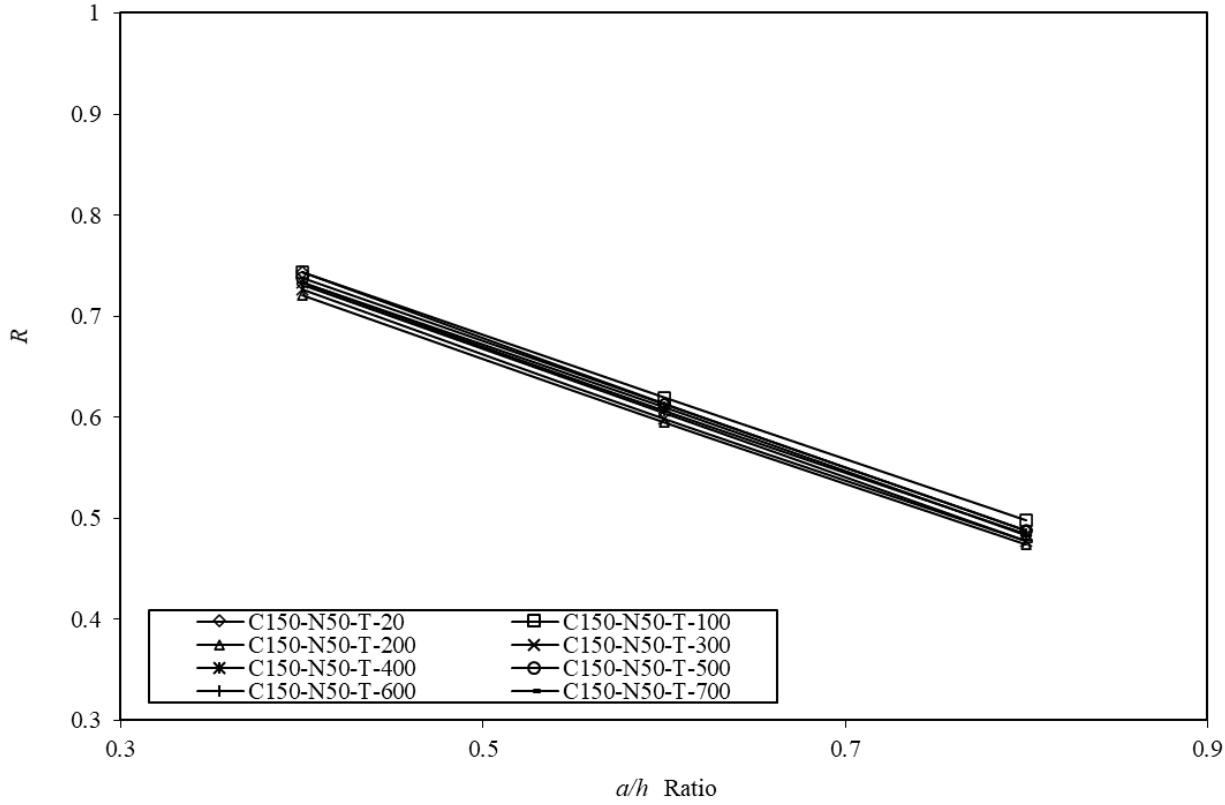

(a) with a/h ratio

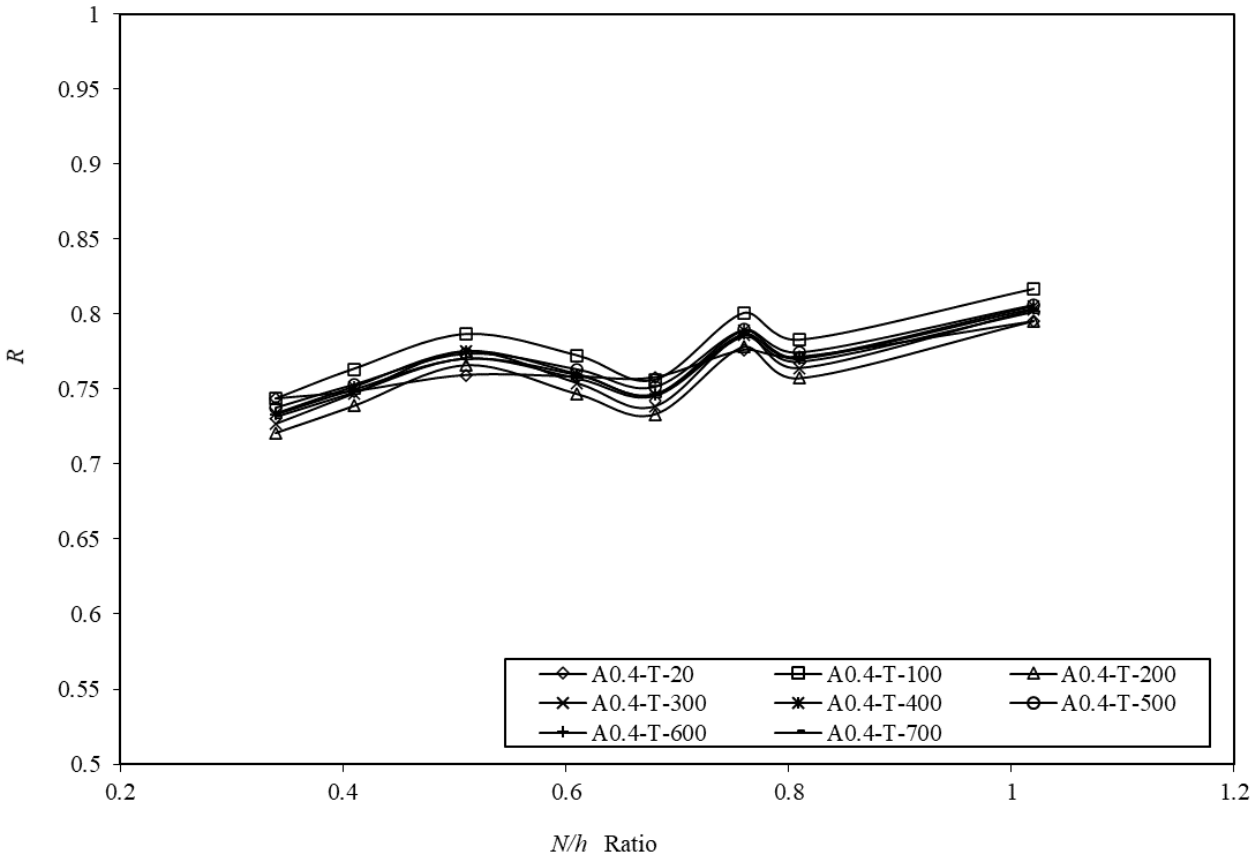

(b) with N/h ratio

Fig. 6 Variation of reduction factors

Table 5
Comparison of the web crippling strength reduction factor with the reduction factor equation proposed by Uzzaman et al. [26]
5(a) ETF-100x45x15-t1.95

			Reduction Factor			Comparison with resistance from Uzzaman et al. [26] ($R/R_{Uzzaman}$)		
Temperature(°C)	N(mm)	N/h	R = P(A0.4)/P(A0)	R = P(A0.6)/P(A0)	R = P(A0.8)/P(A0)	A0.4	A0.6	A0.8
20			0.76	0.65	0.54	1.05	1.07	1.13
100			0.79	0.68	0.58	1.09	1.13	1.20
200			0.77	0.66	0.56	1.06	1.10	1.16
300			0.77	0.67	0.57	1.07	1.11	1.17
400	50	0.51	0.78	0.67	0.56	1.08	1.11	1.17
500			0.77	0.67	0.57	1.07	1.11	1.18
600			0.77	0.66	0.56	1.07	1.10	1.17
700			0.77	0.66	0.56	1.07	1.10	1.16
20			0.78	0.68	0.58	1.03	1.07	1.13
100			0.80	0.70	0.61	1.07	1.11	1.19
200			0.78	0.68	0.59	1.04	1.08	1.16
300			0.79	0.69	0.59	1.05	1.09	1.16
400	75	0.76	0.79	0.69	0.60	1.05	1.09	1.17
500			0.79	0.69	0.60	1.05	1.10	1.17
600			0.79	0.69	0.60	1.05	1.10	1.18
700			0.79	0.69	0.60	1.05	1.09	1.16
20			0.79	0.70	0.61	1.02	1.06	1.13
100			0.82	0.72	0.63	1.04	1.09	1.16
200			0.80	0.70	0.61	1.02	1.06	1.13
300			0.80	0.71	0.62	1.03	1.07	1.13
400	100	1.02	0.81	0.71	0.62	1.03	1.07	1.14
500			0.81	0.72	0.63	1.03	1.08	1.16
600			0.80	0.72	0.63	1.03	1.08	1.16
700			0.80	0.71	0.62	1.02	1.07	1.15

5(b) ETF125x45x15t1.95

			Reduction Factor			Comparison with resistance from Uzzaman et al. [26] ($R/R_{Uzzaman}$)		
Temperature(°C)	N(mm)	N/h	R = P(A0.4)/P(A0)	R = P(A0.6)/P(A0)	R = P(A0.8)/P(A0)	A0.4	A0.6	A0.8
20			0.75	0.63	0.51	1.06	1.06	1.09
100			0.76	0.65	0.53	1.08	1.10	1.14
200			0.74	0.62	0.51	1.04	1.05	1.08
300			0.75	0.63	0.51	1.05	1.06	1.10
400	50	0.41	0.75	0.63	0.52	1.06	1.07	1.10
500			0.75	0.64	0.52	1.06	1.08	1.11
600			0.75	0.63	0.52	1.06	1.08	1.10
700			0.75	0.63	0.51	1.05	1.07	1.09
20			0.76	0.65	0.55	1.03	1.05	1.11
100			0.77	0.67	0.57	1.05	1.08	1.15
200			0.75	0.64	0.54	1.02	1.04	1.10
300			0.75	0.64	0.55	1.03	1.05	1.11
400	75	0.61	0.76	0.65	0.55	1.04	1.06	1.12
500			0.76	0.66	0.56	1.04	1.07	1.13
600			0.76	0.66	0.56	1.04	1.07	1.13
700			0.76	0.65	0.55	1.03	1.06	1.12
20			0.77	0.67	0.57	1.02	1.05	1.11
100			0.78	0.68	0.59	1.03	1.07	1.14
200			0.76	0.65	0.56	1.00	1.03	1.09
300			0.76	0.66	0.56	1.01	1.03	1.09
400	100	0.81	0.77	0.67	0.57	1.02	1.05	1.11
500			0.77	0.67	0.58	1.02	1.06	1.13
600			0.77	0.67	0.58	1.02	1.06	1.13
700			0.77	0.67	0.57	1.01	1.05	1.11

5(c) ETF150x45x15t1.95

			Reduction Factor			Comparison with resistance from Uzzaman et al. [26] (R/ $R_{Uzzaman}$)		
Temperature(°C)	N(mm)	N/h	R = P(A0.4)/P(A0)	R = P(A0.6)/P(A0)	R = P(A0.8)/P(A0)	A0.4	A0.6	A0.8
20			0.74	0.61	0.49	1.06	1.06	1.06
100			0.74	0.62	0.50	1.06	1.07	1.08
200			0.72	0.59	0.47	1.03	1.02	1.03
300			0.73	0.60	0.48	1.04	1.03	1.04
400	50	0.34	0.73	0.61	0.48	1.05	1.04	1.05
500			0.74	0.61	0.49	1.05	1.05	1.06
600			0.73	0.61	0.48	1.05	1.05	1.05
700			0.73	0.60	0.48	1.04	1.04	1.04
20			0.75	0.63	0.52	1.04	1.05	1.08
100			0.75	0.63	0.53	1.04	1.06	1.10
200			0.73	0.61	0.50	1.01	1.01	1.05
300			0.73	0.61	0.51	1.02	1.02	1.05
400	75	0.51	0.74	0.62	0.51	1.03	1.03	1.07
500			0.74	0.63	0.52	1.03	1.05	1.09
600			0.74	0.63	0.52	1.03	1.04	1.08
700			0.74	0.62	0.51	1.02	1.03	1.07
20			0.76	0.64	0.55	1.02	1.04	1.09
100			0.76	0.65	0.55	1.02	1.04	1.10
200			0.73	0.62	0.52	0.99	1.00	1.04
300			0.74	0.62	0.53	1.00	1.00	1.05
400	100	0.68	0.75	0.63	0.53	1.01	1.02	1.07
500			0.75	0.64	0.55	1.01	1.03	1.09
600			0.75	0.64	0.54	1.01	1.03	1.08
700			0.75	0.63	0.54	1.00	1.02	1.07

Table 6
Statistical analysis for determining the applicability of strength reduction factor equation proposed by Uzzaman et al. [26] for CFS C-sections loaded under ETF loading from ambient temperature to elevated temperatures.

		Statistical Parameters R_{FEA}/R_p ((0.90 – 0.60(a/h) + 0.12(N/h))		
Temperature(^{0}C)	Mean, P_m	Coefficient of Variation V_p	Reliability index β	Resistance Factor ϕ
20	1.07	0.03	2.85	0.90
100	1.09	0.04	2.93	0.90
200	1.05	0.04	2.77	0.90
300	1.06	0.04	2.81	0.90
400	1.07	0.04	2.85	0.90
500	1.08	0.04	2.88	0.90
600	1.07	0.04	2.86	0.90
700	1.07	0.04	2.83	0.90

5. Comparison of the reduction factors

The reduction factor equation proposed by Uzzaman et al. [26] for unfastened CFS C-sections with centred web holes under ETF loading was determined (see equation 1). The feasibility of the proposed equation of Uzzaman et al. [26] was assessed in this study for extending its application from ambient temperature to elevated temperatures. Tables 5(a), 5(b) and 5(c) (see Figs. 7(a) and 7(b)) compare the reduction factors determined from the equation 1 for the case of unfastened C-sections with centred web holes at elevated temperatures.

The reliability of the reduction factor equation proposed by Uzzaman et al. [26] for its application at elevated temperatures was also checked. In order to calculate the reliability index, a resistance factor (ϕ) of 0.90 was used. The load combination of 1.2DL + 1.6LL (DL = Dead load, LL = Live load) as mentioned in the NAS specification [28] was used in the reliability study. The mean (M_m) and coefficient of variation (V_m) of the material properties were considered as 1.10 and 0.10, respectively. As can be seen from Table 6, for every specific temperature ranging from 20^0 to 700^0 C, the β (reliability factor) value was greater than 2.5 (see Fig. 8). This is the target reliability index value for CFS structural members and is recommended by the North American specification [29] as the lower limit. This shows that the proposed strength reduction factor equation of Uzzaman et al. [26] is acceptable in determining the effect of circular web holes on the web crippling strength of CFS C-sections at elevated temperatures.

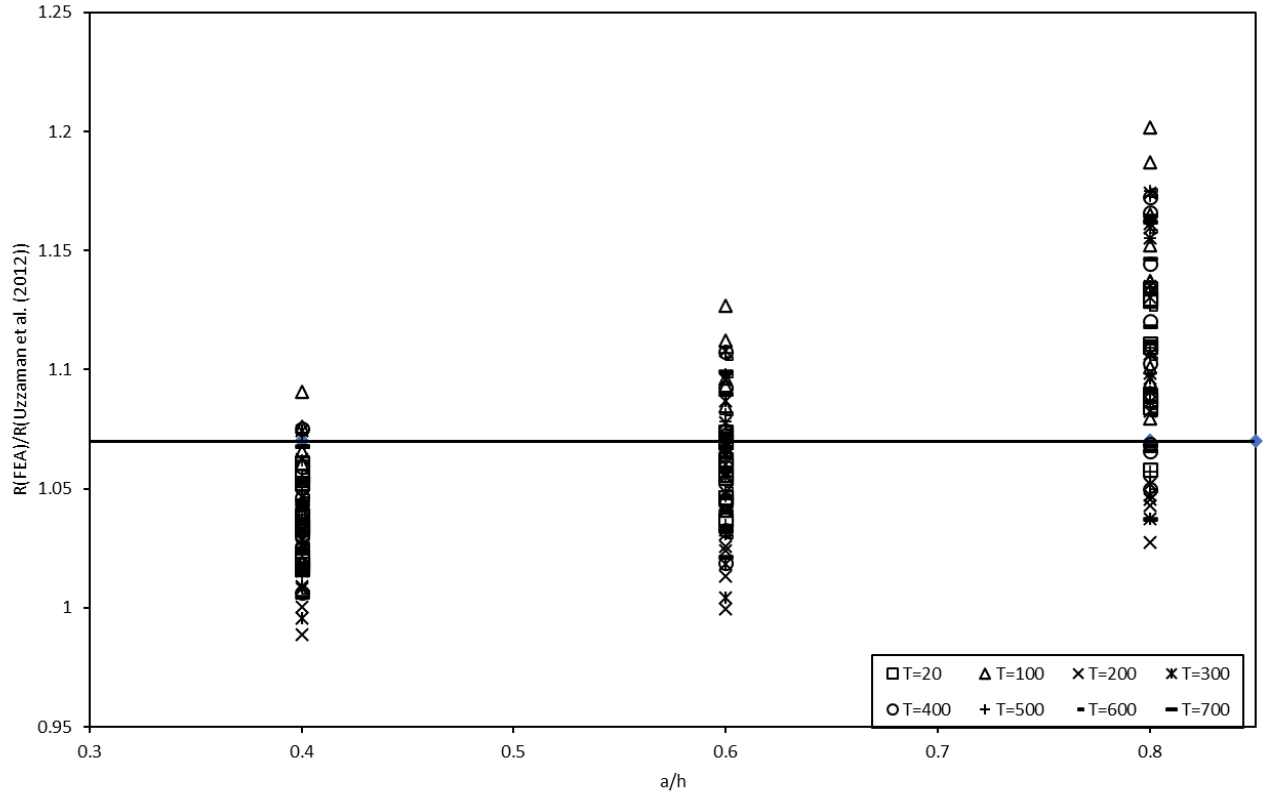

(a) R(FEA)/RUzzaman et al. vs a/h ratio

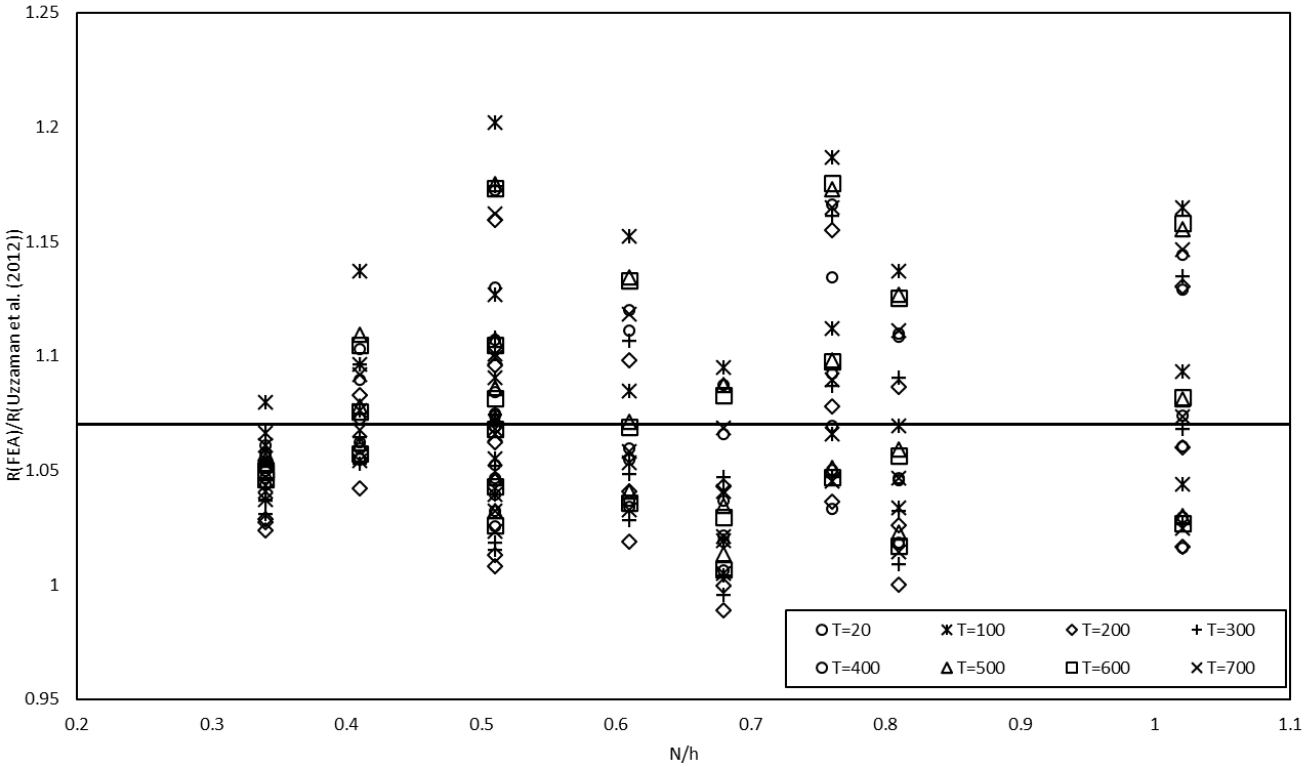

(b) R(FEA)/RUzzaman et al. vs N/h ratio

Fig. 7 Strength reduction factor comparison with centred circular web holes

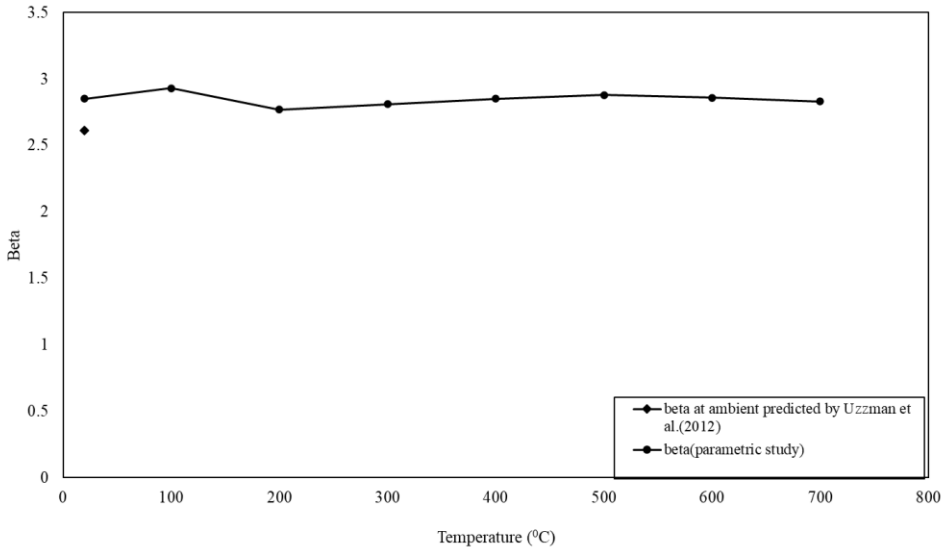

Fig. 8 Comparison of the beta value obtained from the parametric study and the beta value at the ambient temperature by Uzzaman et al. [26]

6. Conclusion

This study investigated the influence of circular web holes and bearing length on the web crippling strength of G250 grade of CFS C-sections when subjected to ETF loading at elevated temperatures. A finite element model was developed for CFS C-sections under ETF loading conditions and validated against the corresponding experimental results available in the literature. The validated finite element model was then used to conduct an extensive parametric study comprising 288 models. The aim of this parametric study was to investigate the effects of different parameters such as the sizes of the web holes, bearing length and temperature ranging from 20 ^{0}C to 700 ^{0}C at an interval of 100 degrees, on the web crippling capacity of CFS C-sections under ETF loading. Both the cases of C-sections with and without web holes were considered.

The parametric study results were then used to assess the applicability of the strength reduction factor equation proposed by Uzzaman et al. [26] for CFS channel-sections with web holes under ETF loading from ambient temperature to elevated temperatures. After statistical analysis in the form of reliability analysis, it was found that the reduction factor equation of Uzzaman et al. [26] is safe and reliable to be used at elevated temperatures.

Notations

a	Diameter of circular web hole;
a/h	Web hole ratio;
b_f	flange width;
b_l	lip width;
d	Depth of cross-section;
E	Young's modulus of elasticity;
FEA	Finite element analysis;
h	Depth of the web's flat portion;
L	Specimen length;
N	Bearing plate length;
N/h	Bearing length ratio;
P_{EXP}	Experimental ultimate web crippling load per web;
P_{FEA}	Web crippling strength per web predicted from FEA;
P_m	Mean;
r_q	Inside fillet radius between web and hole;
r_i	Inside fillet radius of section;
R_{FEA}	Reduction factor obtained from FEA study;
$R_{Uzzaman}$	Reduction factor obtained from Uzzaman et al. (2012);
t	Thickness of the section;
f_u	Static ultimate tensile strength;
f_y	Yield stress;
β	Reliability index;
V_p	Coefficient of variation;
ϕ	Resistance factor;
σ_{true}	True stress;
σ	Engineering stress;
ε	Engineering strain;
$\varepsilon_{true,pl}$	True plastic strain;

References

[1] Javed, F. M., Hafizah , N., Memon , A. S., Jameel , M., & Aslam , M. (2017). Recent research on cold formed steel beams and columns at elevated temperature: A review. Construction and Building Materials, 144, 686-701.
[2] Darcy, G., & Mahendran, M. (2008). Development of a new cold formed steel building system. Advances in Structural Engineering, 11(6), 661-677.
[3] Schafer, B. (2002). Local, distortional and euler buckling of thin-walled columns. Journal of Structural Engineering, 128(3), 289-299.
[4] Roy, K., Lim, J. B., Lau, H. H., Yong, P., Clifton, G., Johnston, R. P., . . . Mei, C. C. (2019). Collapse Behaviour of a Fire Engineering Designed Single-Storey Cold Formed Steel Building in Fires. Thin Walled structures, 142, 340-357.
[5] Uzzaman , A., Lim , J. B., Nash, D., Rhodes , J., & Young , B. (2013). Effect of offset web holes on web crippling strength cold-formed steel channel sections under end-two flange loading condition. Thin Walled Structures, 65, 34-48.
[6] Lian, Y., Uzzaman, A., Lim, J., Abdelal, G., Nash, D., & Young, B. (2017). Effect of Web holes on web crippling strength of cold formed steel channel sections under interior-one-flange loading condition - Part I: Tests and finite element analysis. Thin Walled Structures, 111, 103-12.
[7] Lian, Y., Uzzaman, A., Lim, J., Abdelal, G., Nash, D., & Young, B. (2017). Effect of Web holes on web crippling strength of cold formed steel channel sections under end-one-flange loading condition - Part II Parametric study and proposed design equation. Thin Walled Structures, 111, 103-12.
[8] Gunalan, S., Heva, Y. B., & Mahendran, M. (2015). Local buckling studies of cold formed steel compression members at elevated temperatures. Journal of Constructional Steel Research, 108, 31-45.
[9] Gunalan, S., Mahendran, M. (2019). Experimental study of unlipped channel beams subject to web crippling under one flange load case. Journal of Advanced Steel Construction, 15, 165-172
[10] Elilarasi, K., Kasturi, S., Janarthan, B. (2020). Effect of Circular openings on Web Crippling of Unlipped channel sections under End-two-flange load case. Journal of Advanced Steel Construction, 16, 310-320
[11] Imran, M., Mahendran, M., & Poologanathan, K. (2018). Mechanical properties of cold formed steel tubular sections at elevated temperatures. Journal of Constructional Steel Research, 143, 131-147.
[12] Kankanamge, N. D., & Mahendran, M. (2011). Mechanical properties of cold formed steel at elevated temperatures. Thin Walled Structures, 49, 26-44.
[13] Ranawaka, T., & Mahendran, M. (2009). Experimental study of the mechanical properties of light gauge cold formed steels at elevated temperatures. Fire Safety Journal, 44, 219-229.
[14] Chen, J., & Young, B. (2007). Experimental investigation of cold formed steel material at elevated temperatures. Thin Walled Structures, 45(1), 96-110.
[15] Lim, J.B.P, & Young, B. (2007). Effects of elevated temperatures on bolted moment connections between cold formed steel members. Engineering Structures, 29, 2419-2427.
[16] Landesmann, A., & Camotim, D. (2016). Distortional failure and DSM design of cold-formed steel lipped channel beams under elevated temperatures. Thin Walled Structures, 98, 75-93.
[17] Laim L. Rodrigues Joao Paulo C., Craveiro Helder D. (2016). Flexural behaviour of axially and rotationally re-strained cold-formed steel beams subjected to fire. Thin Walled Structures, 98, 39-47

[18] Kankanamge, N. D., & Mahendran M. (2012). Behavior and design of cold formed steel beams subjected to lateral torsional buckling at elevated temperatures. 61, 213-228.
[19] Gunalan, S., Heva, B. Y., & Mahendran, M. (2014). Flexural-Torsional buckling behaviour and design of cold formed steel compression members at elevated temperatures. Engineering Structures, 79, 149-168.
[20] Ranawaka, T., & Mahendran, M. (2010). Numerical modelling of light gauge cold formed steel compression members subjected to distortional buckling at elevated temperatures. Thin Walled Structures, 48, 334-344.
[21] Feng, M., & Wang, Y. (2003). Structural behaviour of cold-formed thin-walled short steel channel columns at elevated temperatures. Part I experiments. Thin-Walled Structures, 41, 543-570.
[22] ASCE. ((2005)). Minimum design loads for buildings and other structures. American Society of Civil Engineers Standard.
[23] BS EN 1993-1-1 Eurocode 3. Design of Steel Structures. General requirements, British Standards Institutions;2005
[24] BS5950 (1998). Structural use of steelwork in buildings. Part 5 Code of practice for the design of cold-formed sections, London: British Standard Institution
[25] AS/NZS Standards Australia. Cold Formed Steel Structures, AS/NZS 4600:2018, Standards Australia/Standards New Zealand, 2018
[26] Uzzaman, A., Lim, J.B.P., Nash, D., Rhodes, J., & Young, B. (2012). Cold-formed steel sections with web openings subjected to web crippling under two-flange loading conditions - Part II: Parametric study and proposed design equations. Thin-Walled Structures, 56, 79-87.
[27] Uzzaman, A., Lim, J.B.P, Nash, D., Rhodes, J., & Young, B. (2012). Cold-formed steel sections with web openings subjected to web crippling under two-flange loading conditions - Part I: Tests and Finite element analysis. Thin-Walled Structures, 56, 38-48
[28] ANSYS. (2017). User's Manual, revision 17.0. Swanson Analysis System.
[29] NAS, North American Specification for the design of cold-formed steel structural members. AISI S100-2007, AISI Standard. American Iron and Steel Institute;2007.